

Physical mechanisms of contact-electrification induced photon emission spectroscopy from interfaces

Yang Nan^{1,2,§}, Jiajia Shao^{1,2,§}, Ding Li^{1,2}, Xin Guo^{1,2}, Morten Willatzen^{1,2} (✉), and Zhonglin Wang^{1,2,3} (✉)

¹ Beijing Institute of Nanoenergy and Nanosystems, Chinese Academy of Sciences, Beijing 101400, China

² School of Nanoscience and Technology, University of Chinese Academy of Sciences, Beijing 100049, China

³ Georgia Institute of Technology, Atlanta, GA 30332, USA

[§] Yang Nan and Jiajia Shao contributed equally to this work.

© Tsinghua University Press 2023

Received: 4 February 2023 / Revised: 9 March 2023 / Accepted: 16 March 2023

ABSTRACT

Photon emission during contact electrification (CE) has recently been observed, which is called as CE-induced interface photon emission spectroscopy (CEIIPES). Physical mechanisms of CEIIPES are essential for interpreting the structure and electronic interactions of a contacted interface. Using the methods of density functional theory (DFT) and time-dependent DFT (TDDFT), it is confirmed theoretically that the spectrum of emitted photons is contributed from electron transfer and transition during CE. Specifically, the excited electrons from higher energy state in one material may transfer to a lower energy state of another material followed by a transition; and/or some unstable excited electrons at a higher energy level of one material may transit to a lower energy state of itself, both of which result in CEIIPES. Furthermore, the CE-induced interface absorption spectrum (CEIIAS) has been demonstrated, due to the intermolecular electron transfer excitation.

KEYWORDS

spectroscopy, contact electrification (CE), time-dependent density functional theory (TDDFT), CE-induced interface photon emission spectroscopy (CEIIPES), CE-induced interface absorption spectrum (CEIIAS), polymers

1 Introduction

In the last few decades, spectroscopy has emerged as one of the most essential methods for analyzing the electronic structure of a system [1–5]. This is due to the fact that an atom or molecule can only exist in certain discrete energy level according to Bohr's theory from 1913 [6]. Electrons can jump between allowed discrete energy states via photon emission or absorption as described by the time-independent Schrödinger equation

$$\hat{H}(r, R)|\Psi(r, R)\rangle = E|\Psi(r, R)\rangle \quad (1)$$

where $\hat{H}(r, R)$ is the Hamiltonian of the system with r and R being the locations of the nuclei and electrons, E represents energy level, and $\Psi(r, R)$ is the wave function representing the state of the system, respectively. The frequency of the light (ν) is determined by the energy difference (ΔE) between two eigenstates divided by Planck's constant

$$h\nu = hc/\lambda = \Delta E \quad (2)$$

where h is Planck's constant, c is the speed of light in vacuum, and λ is the wavelength of the light, respectively. For better studying the electronic structures of a system by spectroscopy, endeavors have been made to excite this system using different methods such as photon emission induced by light, flame, plasma, arc, or spark [7, 8].

Recently, photon emission related to contact electrification (CE) has been observed as a new optical spectroscopy method for

studying electronic transitions according to the energy dissipation during electron transfer and has been characterized as atomic featured spectrum in the experiment. This method is designated CE-induced interface photon emission spectroscopy (CEIIPES) [9]. Different from triboluminescence associated with air discharge [10, 11], CEIIPES reflects electron transition because of CE. The motion of electrons provides abundant information about the energy levels or orbitals of atoms or molecules, which allows us to develop a theoretical understanding of their electronic structures at an interface. Therefore, understanding the physical process of CEIIPES is essential for studying electronic interactions between solids, liquids, and gases.

However, the physical process of CEIIPES is ambiguous due to limitations of atomic spectroscopy in describing complex systems of atoms compared with single atoms. For a contact system, the case becomes more complicated as the combination of atoms into molecules leads to a rich variety of energetic states and transition strengths between these states. For this reason, it appears difficult to deduce the physical process of electron transition between unique energy levels using solely atomic spectroscopy. In this circumstance, molecular spectra can provide sufficient information not only for the spectra generated by the vibration and rotation of the nuclei [12], but also for the spectra of the transitions between the aforementioned energetic states. The energy of a certain molecular state (E_{tot}) can be separated into three contributions according to the Born–Oppenheimer approximation

Address correspondence to Morten Willatzen, mortenwillatzen@binn.cas.cn; Zhonglin Wang, zlwang@gatech.edu

$$E_{\text{tot}} = E_{\text{ele}} + E_{\text{vib}} + E_{\text{rot}} \quad (3)$$

where E_{ele} , E_{vib} , and E_{rot} represent the energies of electronic interaction, vibration, and rotation, respectively. To identify the transition process when two materials are brought into contact, E_{vib} and E_{rot} are not considered due to the differences in timescale (the timescales of E_{ele} , E_{vib} , and E_{rot} are around 10^{-15} , 10^{-14} , and 10^{-13} s, respectively) according to the motions of molecules [13, 14]. Thus, the spectra induced by electron transition can be obtained independently for vibration or rotation. Furthermore, interpreting a spectroscopic experiment necessitates detailed first-principles computations to determine which transition process of the given system is accountable for spectra. Most importantly, understanding electronic structure and how it manifests itself in the spectra can give insights into any electron transition process for all systems, rather than a single system. Fortunately, the development of density functional theory (DFT) [15, 16] and time-dependent DFT (TDDFT) [17–20] provides support to investigate electronic structures [21–24] in various systems where the electrons are treated by first-principles using quantum mechanics. DFT has been implemented in various CE systems and manifests satisfactory performance in the description of electron transfer and transition [25, 26]. Using TDDFT, a correspondence between time-dependent charge density and the external time-dependent potential and initial wavefunction is established (details could be found in Supplementary Note 1 in the Electronic Supplementary Material (ESM)), allowing one to obtain and address the evolution of interacting electrons at excited states (S_1 , S_2 ...) and the corresponding spectra [27, 28], which can provide theoretical expressions linking electron transition processes and spectroscopy.

In this work, we used such methods to investigate the physical process of CEIPES by studying the motion of electrons (transfer and transition). It is demonstrated that the governing processes for CEIPES stem from electron excitation to higher energy levels in one material followed by a transition to lower energy levels of another material, i.e., the contacting material. We discovered that the direction of electron transfer between polymers is directly correlated with the electrostatic potential (ESP), based on which we proposed a new parameter. This parameter not only provides a favorable description of electron transfer for the polymers considered in the present work, but it is also applicable to previously reported polymer/metal CE and may be transferable to other CE systems, such as CE in polymer/dielectric and water/oil systems. Besides, the amount of electron transfer is confirmed to be influenced by polymer length, polymer ordering, polymer saturation, and contact distance. Furthermore, electron transfer dominates the absorption spectra in the relatively lower excited states, whereas absorption spectra in the higher excited states are primarily attributed to electronic structure rearrangement according to the charge transfer spectrum (CTS). This indicates that the energy provided by CE for electron transition is too small to invoke electron excitation to high energy level states. Based on this, we studied the physical process of CEIPES by combining the analysis of electronic structure with a comparison of emission spectra of contacted polymers and independent polymers. Moreover, we presented a method for deciphering emission spectra induced by CE or contacted matter itself by comparing the peak position in the spectra for a better understanding and implementation of CEIPES in future experimental analyses.

2 Results and discussion

2.1 Contact electrification at polymer/polymer interface

Studying the motions of electrons is essential to understanding

CEIPES, since a portion of energy dissipation in the process of electron transfer due to CE is characterized as photon emission due to electron transfer and gives birth to CEIPES. Electron transfer normally occurs immediately after two polymers come into contact, and opposite charges accumulate at different surfaces (Fig. 1(a)). Polymers have satisfied performance in CE mainly by virtue of their diverse repeat units and functional groups (Fig. 1(b) and Fig. S1 in the ESM) [22, 29, 30]. The diversified repeat units and functional groups contribute to the accessible modifiability of polymers. For example, polyvinylidene fluoride (PVDF) is obtained as a consequence of substituting half of the fluorine atoms of polytetrafluoroethylene (PTFE) by hydrogen atoms (Fig. 1(b)). The modifiability of polymers implies adjustment of their molecular orbitals (MOs) (Fig. 1(c) and Table S1 in the ESM) and intrinsic properties like vertical ionization potential (VIP), vertical electron affinity (VEA), Mulliken electronegativity (MEN) (Fig. 1(d) and Table S2 in the ESM, the interpretations of these parameters are findable in Supplementary Note 2 in the ESM), and ESP (Figs. 1(e)–1(g), and Fig. S2 and Supplementary Note 3 in the ESM), which is constructive to the utilization of polymers in CE. According to the calculations of frontier MOs (Fig. 1(c) and Table S1 in the ESM), the lowest unoccupied molecular orbital (LUMO) energies of PVDF and PTFE are 1.17 and -0.39 eV, respectively. PVDF and PTFE have highest occupied molecular orbital (HOMO) energy values of -8.21 and -9.16 eV, respectively. Although the chain topologies of polyethylene (PE), PVDF, and PTFE are comparable (Fig. 1(b)), PE has the largest HOMO energy (-7.92 eV), LUMO energy (2.46 eV), and HOMO–LUMO gap (10.38 eV). Such differences caused by different functional groups can also be found in other polymers (Tables S1 and S2 in the ESM). To provide a quantitative assessment of ESP, we proposed a parameter based on the molecular surface area in each ESP range written as

$$R_{\text{pn}} = \frac{A_{\text{positive}}}{A_{\text{negative}}} \quad (4)$$

where A_{positive} and A_{negative} are the surface areas of positive and negative regions in the range of ESP respectively, and can be obtained by Multiwfn software directly.

According to the electron cloud overlap model [31–34], electron transfer is caused by the overlap of electron wavefunction when two materials are brought into contact. The overlap area of the electron cloud when PE and PTFE are in contact with each other is estimated by the translucent green area in Fig. 2(a), which determines the electron transfer strength between the two polymers. The electron density difference (EDD) was obtained before and after the PE was contacted with PTFE, finally providing an intuitive picture of electron transfer (Fig. 2(b)). The blue and red bubbles reflect the increase and reduction of electrons, respectively. Obviously, red bubbles are mostly found on PTFE while blue bubbles are mainly distributed near PE, demonstrating that electrons are transferred from PTFE to PE (Fig. 2(b)). More precisely, the electron density decreases mostly on the fluorine atoms, whereas the electron density increases primarily on the hydrogen atoms (inset in Fig. 2(b)). It is noteworthy to observe that PE receives electrons when it contacts with other listed polymers (Fig. 2(c) and Table S3 in the ESM). On the contrary, PTFE gets positively charged after contacting with other polymers except for PVDF (Fig. 2(c) and Table S3 in the ESM). We find that the directions of electron transfer between polymers are strongly related to their R_{pn} values (Fig. S3 in the ESM), while the parameters that assess the electron affinity like VIP, VEA, and MEN, as well as material properties such as LUMO and HOMO, are unable to adequately describe electron transfer. As electrons prefer to transfer from a negative potential to a positive potential,

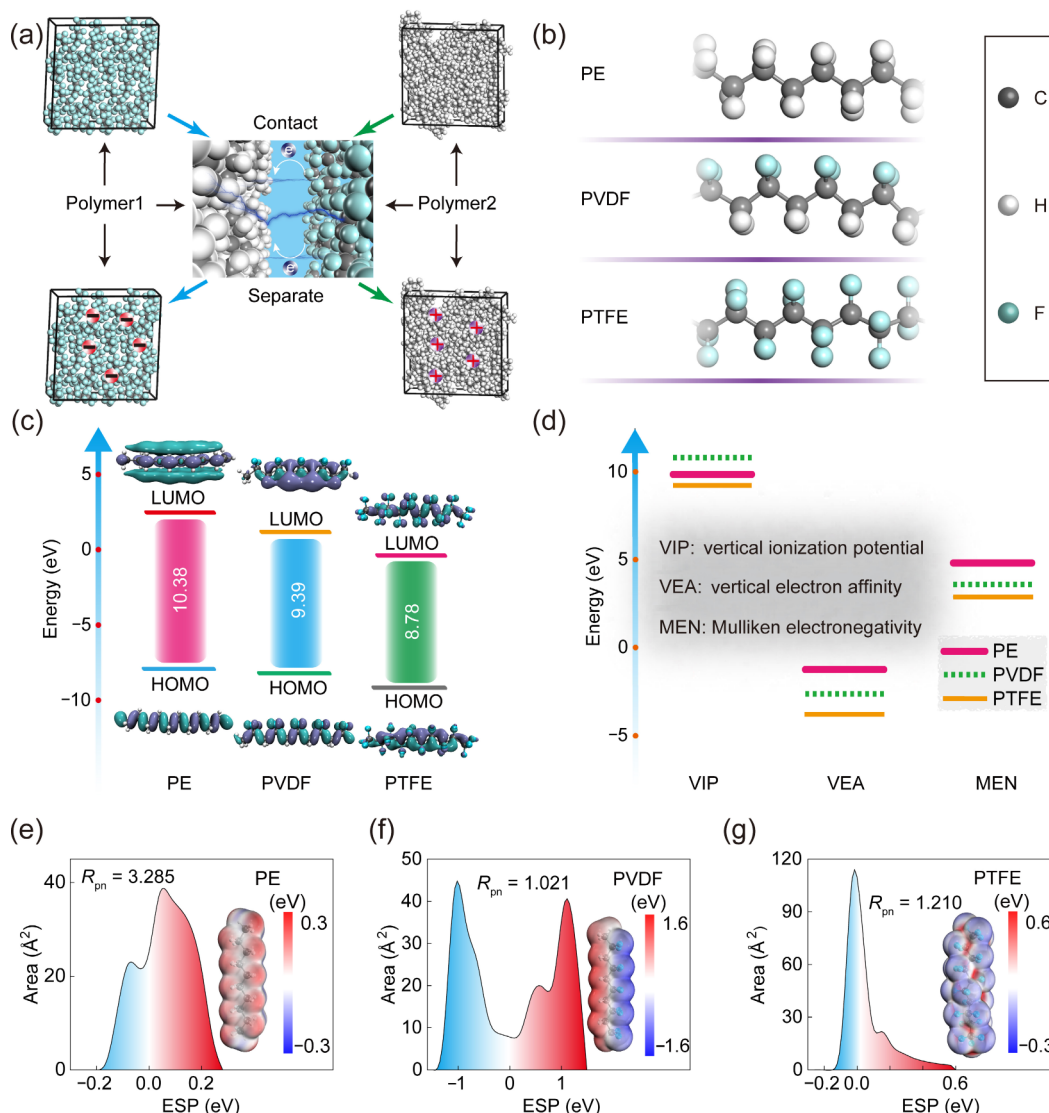


Figure 1 Chemical structures and theoretical calculations. (a) Diagram showing contact electrification at a polymer/polymer interface. (b) Chemical structures of PE, PVDF, and PTFE, respectively. (c) Simulated frontier orbital energy levels and the calculated HOMO–LUMO gaps of PE, PVDF, and PTFE. The insets show the MO diagrams. (d) The values of VIP, VEA, and MEN for PE, PVDF, and PTFE. (e)–(g) ESP distribution and area in each electrostatic potential range of PE, PVDF, and PTFE, respectively.

PE has the largest R_{pn} while PVDF has the smallest R_{pn} (Fig. S3 in the ESM), causing PE to obtain electrons from other polymers and PVDF to donate electrons to other polymers. And the order of R_{pn} values is consistent with the direction of electron transfer between polymers (Fig. S3 and Table S3 in the ESM). Moreover, electron transfer will cause the electronic structure to rearrange in order to reach a new stable state. Taking the PE&PTFE pair as an example, we analyzed the charge variations of selected atoms (Fig. 2(d)). Charge variations occur at atoms far from the contact interface owing to the rearrangement of electronic structure. Even the same atoms at different positions undergo different charge changes to reach a new stable state (some fluorine atoms of PTFE are positively charged and some are negatively charged, same for hydrogen atoms in PE). Carbon atoms are positively charged in PE while negatively charged in PTFE because of different functional groups (Fig. 2(e)).

In addition to the influence of the factors mentioned above, the interactions between polymers are remarkable. An independent gradient model based on Hirshfeld partition (IGMH) (Supplementary Note 4 in the ESM) that relies on Multiwfn software was used to investigate the specific molecular interactions between PE and PTFE (Figs. 2(f) and 2(g), and Fig. S5 in the ESM). The results show that only van der Waals (vdW) forces are

responsible for CE of the two polymers, without any bond formation and breakage. This reveals that the mechanism of CE between polymers involves electron transfer rather than chemical processes, which is quite different from the dangling bond driven mechanism of polymer/metal CE [35].

2.2 Influencing factors on electron transfer

We analyzed electron transfer of four potential arrangements between PE and PTFE: (1) PE and PTFE are parallel with each other, (2) PE and PTFE are vertical to each other, (3) PE is perpendicular to the PTFE chain, and (4) PTFE is perpendicular to the PE chain, respectively, aiming to consider the variety of molecular chain arrangements in polymers (Fig. 3(a)). The electron transfer of PE and PTFE for parallel ordering has the largest value among the other three arrangements due to the largest contacting area, whereas the electron transfer of PE and PTFE for vertical ordering has the smallest value, demonstrating that parallel ordering makes the main contribution to CE at polymer/polymer interface. Moreover, the electron transfer values of the other two arrangements, PE perpendicular to PTFE chain and PTFE perpendicular to PE chain, are similar and both larger than that of vertical ordering.

Then we studied the relationship between contact distance and

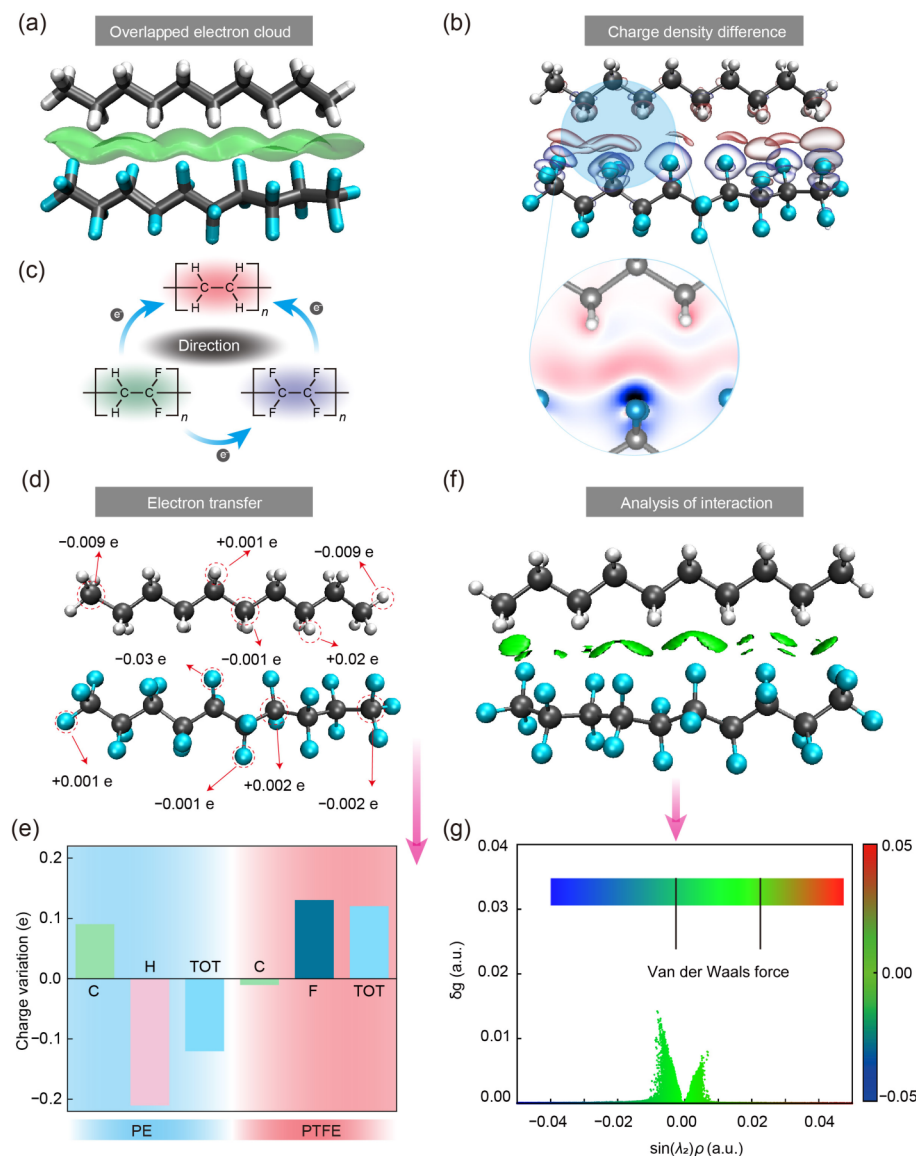


Figure 2 Electron transfer and interaction analysis. (a) The electron cloud overlap (transparent green area) when PE and PTFE are brought into contact with each other. (b) Electron density difference before and after PE and PTFE contacting with each other. Inset indicates the planar average electron density difference of the amplified area. (c) The directions of electron transfer among PE, PVDF, and PTFE when two of them are in contact. (d) The charge differences of selected atoms after PE and PTFE are in contact. (e) The charge variations of each element and total after PE and PTFE are in contact. (f) The interaction analysis of contacted PE and PTFE in parallel ordering. (g) The scatter map between $\sin(\lambda_2)\rho$ and δg . Inset denotes the common interpretation of coloring method of mapped function $\sin(\lambda_2)\rho$. Blue represents strong attraction, green represents van der Waals forces, and red represents strong repulsion, respectively. δg is the sum of the interactions of a system which contain the interactions of interfragment and intrafragment, and ρ is the electronic density.

electron transfer (Fig. 3(b) and Fig. S6 in the ESM). The system energy reduces when the interface distance approaches the equilibrium state (about 2.0 Å in Fig. 3(b) and 2.5 Å in Fig. S6 in the ESM) due to the weakening of repulsive force at the contact region (the red areas in Fig. 3(b) and Fig. S6 in the ESM). As the contact distance increases continuously, the attractive force dominates the non-contact region (the blue areas in Fig. 3(b) and Fig. S6 in the ESM), causing the system energy to rise initially before stabilizing. Nevertheless, electron transfer decreases with increasing contact distance not only in the contact region but also in the non-contact region. This can be well interpreted by the electron cloud overlap model. When two polymers come into close contact (1.5 Å), we observe that a considerable portion of the electron cloud overlaps (top insets in Fig. 3(b) and Fig. S6 in the ESM), leading to a large electron transfer. The overlapping area of the electron cloud diminishes as the contact distance increases (middle inset in Fig. 3(b)), resulting in a weakening of electron transfer. Even in non-contact region, there are overlapping areas of the electron cloud, causing electron transfer (middle inset in

Fig. S6 in the ESM). When there is no electron cloud overlap, electron transfer ceases. After that, we fixed a contact distance and changed the length of PTFE to evaluate the effect of length on electron transfer (Figs. 3(c) and 3(d)). Then, we used the number of C atoms to represent the length of PTFE. It turns out that electron transfer is proportional to the length of parallel ordering, owing to the increase in contact area, or in other words, due to the increase in electron cloud overlap, but the influence of length on vertical ordering is negligible (Fig. 3(e)). The impact of saturation on electron transfer was also investigated. Unsaturation of polymers may be caused by the polymer itself or as a result of atom loss during the friction in CE, and the saturated polymer ($C_{10}H_{22}$ named as PE1 and $C_{10}F_{22}$ named as PTFE1) has now become an unsaturated polymer ($C_{10}H_{21}$ named as PE0 and $C_{10}F_{21}$ named as PTFE0). As a result, the by-products of dangling bonds are created (Fig. 3(f)) [26, 35, 36]. Obviously, electron transfer is dramatically influenced by the saturation of polymers (Fig. 3(g)). The electron transfers of PE1&PTFE0 and PE0&PTFE1 are less than that of PE1&PTFE1, indicating electron transfer is hindered

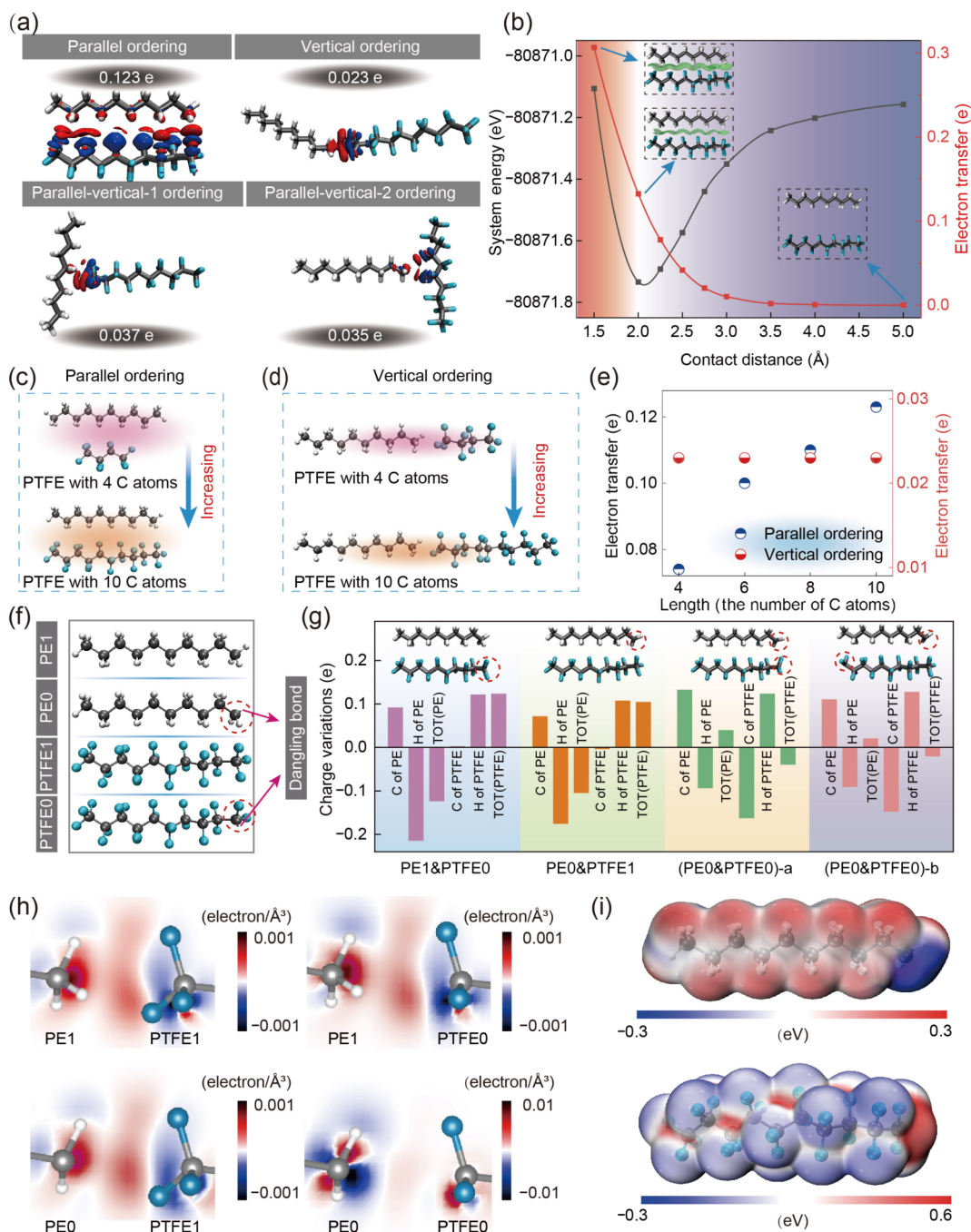


Figure 3 Factors affecting electron transfer. (a) Four potential orderings of PE and PTFE when they are brought into contact and the corresponding transferred electrons. (b) The system energy and electron transfer at different contact distances. Insets show the electron cloud overlap at different contact distances. Configurations of PTFE with different lengths in contact with the same PE chain in (c) parallel ordering and (d) vertical ordering. (e) The relationship between the electron transfer and different lengths of PTFE in contact with PE in the forms of parallel ordering and vertical ordering, respectively. (f) The configurations of saturated PE (PTFE) and unsaturated PE (PTFE). (g) The charge variations of each element and total after saturated (unsaturated) PE and saturated (unsaturated) PTFE are in contact. (h) The planar electron density differences for polymers with different saturations in contact, which are PE1&PTFE1, PE1&PTFE0, PE0&PTFE1, and PE0&PTFE0. (i) The ESP distributions of unsaturated PE and PTFE.

due to the loss of atoms. Surprisingly, the direction of electron transfer is reversed in the cases of both (PE0&PTFE0)-a and (PE0&PTFE0)-b.

To better understand these phenomena, we calculated EDDs of these contacted models (Fig. 3(h)) as well as ESPs of PE0 and PTFE0 (Fig. 3(i)). The results show that the loss of a hydrogen atom at the end of PE exposes a negative region, whereas the lack of a fluorine atom exposes a positive area of PTFE which is unfavorable to electron transfer from PE to PTFE and reduces the amount of electron transfer as a consequence. Furthermore, the calculated R_{pn} values of PE0 and PTFE0 are 2.80 and 2.93, respectively, providing a good agreement to the direction of

electron transfer. In addition, the utilization of surface electrostatic potential to interpret CE is applicable to other systems. For example, previous work [35] held that the dangling bond of PTFE is crucial for electron transfer for metal/polymer CE on the basis that electron transfer is considerably larger for unsaturated PTFE contact with metal than saturated PTFE contact with metal. However, this conclusion is not applicable to our earlier work with water/polymer CE [22], and it is not applicable to this work either. The truth is that metals normally have lower R_{pn} values than polymers, which leads to electron transfer from the metal to the polymer. When PTFE loses a fluorine atom, its R_{pn} becomes larger as mentioned above than when it is saturated, causing a sudden

electron transfer from the metal to PTFE. We predict that the combination of the electron cloud overlap model and R_{pn} describes well the mechanism of CE and has the potential to be applicable to CE in all systems. To be more specific, R_{pn} describes the direction of electron transfer well, while the electron cloud overlap model provides a satisfying description of the amount of electron transfer. We predict that the change of electronic structure is the main factor for CE, and tribocharges that originate from being delivered by electron transfer [37, 38], ion transfer [39, 40], or even material transfer [41, 42] are the factors that influence the electronic structures, where electron transfer is dominant due to its small timescale. As the ions or materials are transferred, the electrons can quickly find their equilibrium states. As is to say, ion transfer or material transfer could accelerate electron transfer. However, this prediction needs further examination.

2.3 CE-induced absorption spectra

Wang's group has characterized emitted photons in the process of electron transfer, providing evidence for electronic transitions

during CE [9]. However, this process is not entirely clear due to a weak understanding of the electronic structure of the excited states in experiments. The electronic structure of excited states is quite different from that near the ground states (S_0). To investigate this electronic excitation process, we first calculated the absorption spectra for contacted PE&PVDF, PE&PTFE, and PVDF&PTFE (Fig. 4(a)). The absorption spectra are chosen to be studied first for the following reasons: Calculating the absorption spectra allows us to calculate numerous excited states at the same time, which is useful for studying the range of excited states where electron transfer has the most influence on the spectra. On the other hand, the calculation of the absorption spectra does not involve the structure optimization of the excited state, which can reduce simulation costs. The absorption spectra are calculated by broadening the vertical energy difference from the ground state to each excited state by Gaussian function (details are available in Supplementary Note 5 in the ESM) [18]. And the unit of absorption spectra (which is also applicable to emission spectra in the following section) is the arbitrary unit, suggesting that only the

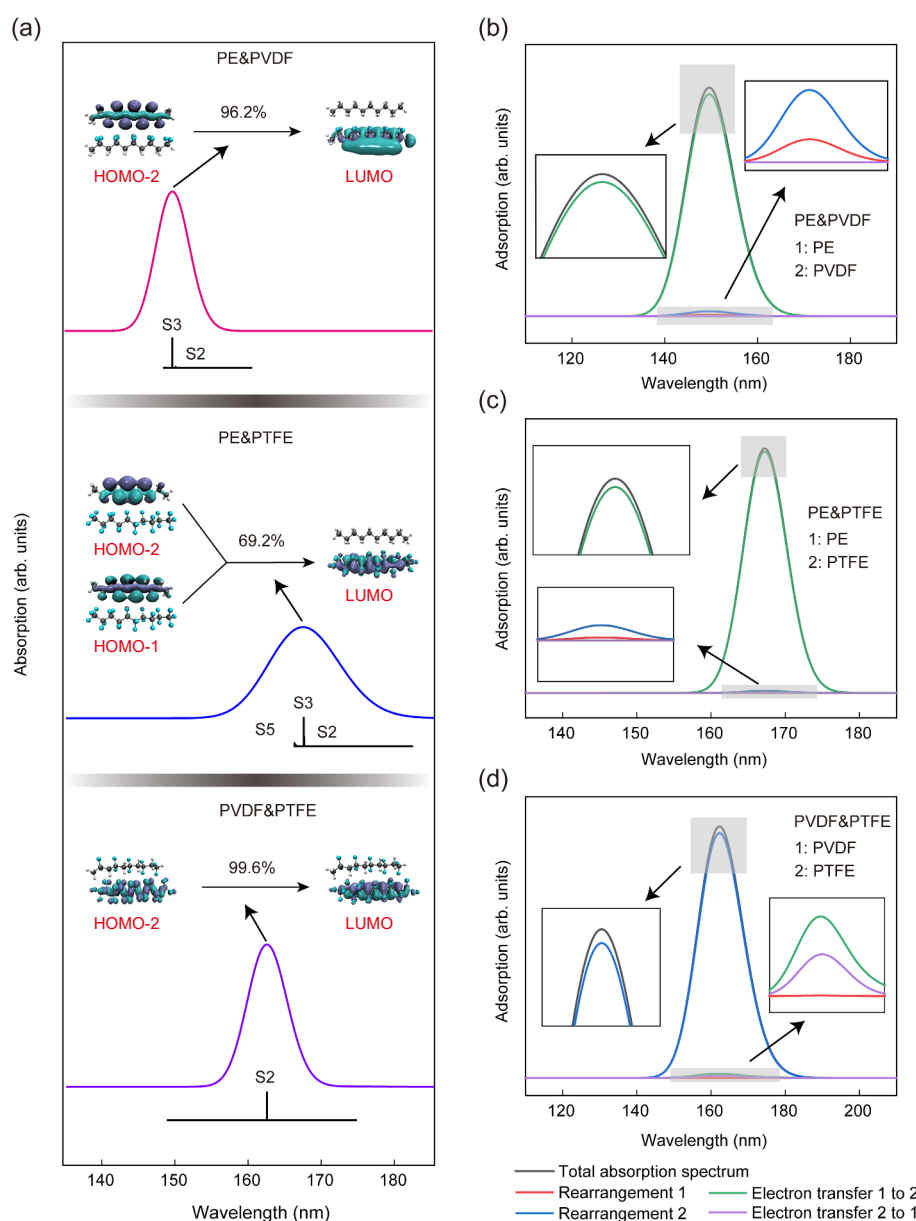


Figure 4 Contact electrification induced absorption spectra and charge transfer spectra. (a) The absorption spectra of contacted PE&PVDF, PE&PTFE, and PVDF&PTFE, and the main contribution excited states to the spectral peaks. The main contribution molecular orbital maps of the main excited states are displayed in insets. (b) The charge transfer spectra of the first 5 excited states when PE and PVDF contacting with each other. (c) The charge transfer spectra of the first 5 excited states when PE and PTFE are in contact. (d) The charge transfer spectra of the first 5 excited states when PVDF and PTFE are in contact.

spectral shape and peak position are meaningful. The absorption spectrum of PE&PVDF is mostly composed of the electronic excitation transition of S3, which is provided mainly by the electronic transition from HOMO-2 to LUMO (Fig. 4(a)). The absorption spectrum of PE&PTFE is dominated by S3, however, this electronic transition state is predominantly given by both HOMO-2 and HOMO-1 to LUMO. It is straightforward to discern that the donor molecular orbital and the acceptor molecular orbital are located on distinct molecules for the above-mentioned electronic excited states (insets in Fig. 4(a)). Differently, the donor and acceptor molecular orbitals of the principal contributing electronic excited state S2 (HOMO-2 to LUMO) for PVDF&PTFE absorption spectrum are all identified at PTFE. It seems that intermolecular electron transfer drives the absorption spectra of PE&PVDF and PE&PTFE, whereas that of PVDF&PTFE is influenced mostly by electronic rearrangement.

To further understand the nature of electron excitation in terms of intramolecular electronic structure redistribution and intermolecular electron transfer, the CTS [43] (Supplementary Note 5 in the ESM) method was utilized for each absorption spectrum. As can be observed, electron transfer (green line) accounts for practically the whole optical absorption of PE&PVDF (black line), whereas electronic structure redistributions of each polymer in excited state account for a small fraction and can be ignored (Fig. 4(b)). The decomposed absorption spectra of PE&PTFE produce a comparable result, demonstrating that electron transfer between two polymers dominated the total absorption spectrum (Fig. 4(c)). However, the total absorption spectrum identified in PVDF&PTFE is ascribed to an electronic structural rearrangement inside the PTFE, since the blue line depicting electron redistribution in the PTFE fragment is close to the total absorption spectrum (black line) of PVDF&PTFE (Fig. 4(d)). These findings are consistent well with the orbital contribution analysis discussed earlier (Fig. 4(a)).

It is worth noting that the calculations of electron excitation also include electron transfer excitation (Fig. S7(a) in the ESM) and local excitation (Fig. S7(b) in the ESM), with the former indicating that the distribution regions of electrons changed significantly after excitation and the latter suggesting that the distribution regions of electrons before and after excitation have no obvious change. And electron transfer excitation comprises intramolecular electron transfer excitation as well as intermolecular electron transfer excitation. Only the absorption spectra produced mostly by intermolecular electron transfer excitation can be classified as CE-induced interface absorption spectrum (CEIIAS). The calculated absorption spectra for the PVDF&PTFE pair are mostly contributed by local electron excitation of only one of the materials and cannot be considered as CEIIAS (Fig. 4(d)), whereas the contacted pairs, such as PE&PVDF and PE&PTFE, whose absorption spectra are solely contributed by intermolecular electron transfer (Figs. 4(b) and 4(c)) can be considered as CEIIAS and studied. Furthermore, the absorption spectra in this section are calculated using the first 5 excited states to guarantee that the spectra are almost entirely contributed by electron transfer, because the influence of electronic structure redistribution increases as the number of calculated excited states increases (Fig. S8 in the ESM). The fractions of electronic structure rearrangement in absorption spectra of PE&PVDF, PE&PTFE, and PVDF&PTFE in the first 10 excited states and in the first 50 excited states dominate the absorption spectra (blue curves in Figs. S8(a)–S8(e) in the ESM, and blue and red curves in Fig. S8(f) in the ESM), which cannot be regarded as CEIIAS. As a result, CEIIAS occurs mostly at lower excited states, which might be due to the fact that the excitation energy provided by CE makes it difficult for electrons to reach a higher energy level. Similarly, electronic structural rearrangement

in more than the first 10 excited states dominates absorption spectra in PE&polyethylene terephthalate (PET), PE&polypropylene (PP), PE&Kapton, and PE&Nylon66 pairs (Fig. S9 in the ESM). Based on this, the discussion of CE-induced emission spectra in the next section will focus on relatively lower excitation states.

2.4 CE-induced emission spectra

There are three possible physical processes of CEIIPES: (1) Electrons are excited to the higher energy level and followed by transitioning to a lower energy level of the same material; (2) electrons are excited to the higher energy level of another material and followed by transitioning to the lower energy level; and (3) electrons are excited to the higher energy level in one material then directly transitioned to the lower energy level of another material. However, regardless of the physical process, the experiment yields the same result, i.e., the detection of emitted photons. To characterize and figure out the physical process of CEIIPES, a more demanding study needs to be performed. Here, we performed TDDFT method to calculate emission spectra of various contact pairs by obtaining the vertical energy difference between the ground state and the optimized excited state [18, 44]. Similarly to CEIIAS, only the spectra induced by transferred electrons undergoing transition during CE can be regarded as CEIIPES, whereas emission spectra induced by electronic structure redistribution should be regarded as a separate instance to analyze. Additionally, the combination of atoms into molecules leads to the creation of diverse energy levels and therefore, describing electrons as transferring between materials instead of between atoms is more precise.

Fortunately, the oscillator strength (Supplementary Note 1 in the ESM) of PE is zero in both S1 and S4, suggesting that PE has no emission spectra in either $S1 \rightarrow S0$ or $S4 \rightarrow S0$, making PE an excellent probe material for examining the mechanism of CEIIPES (Table S4 in the ESM). In addition, the emission spectra of PVDF and contacted PE&PVDF in $S1 \rightarrow S0$ and $S4 \rightarrow S0$ were also calculated, respectively (Fig. 5(a)). Unlike PE, the emission spectra of PVDF in $S1 \rightarrow S0$ and $S4 \rightarrow S0$ display different locations and intensities. The CE-induced emission spectrum of PE&PVDF, on the other hand, is only observed in $S4 \rightarrow S0$ and has an independent peak location, whereas the spectrum in $S1 \rightarrow S0$ vanishes. In addition, the excitation energy of PE&PVDF in $S4 \rightarrow S0$ is 6.922 eV, which is larger than that of PVDF (6.284 eV), indicating that CE provides external energy for electrons to jump to a higher energy level. To gain additional insights into the CE-induced emission spectra, we performed electron–hole analysis [45] (details are mentioned in Supplementary Note 6 in the ESM, and results are listed in Tables S5 and S6 in the ESM) on the relaxed S1 and S4 for PE&PVDF (Fig. 5(b)). As can be seen, PE contains almost all of the holes (yellow), indicating that PE accounts for all electrons in both S1 and S4. The electrons (blue) are distributed in both PE and PVDF, with the distribution of electrons in PE being larger in S1 while smaller in S4. In addition, the electrons in PVDF have the highest ratio in comparing the hole and the redistribution, suggesting that the electrons of PVDF are almost entirely contributed by PE.

Based on the results and the discussion above, we can determine the physical process of CEIIPES. We notice that electrons of PVDF are almost entirely contributed by PE in S1 and S4. If electrons are excited from PE to the higher energy level of PVDF and subsequently transferred to the lower energy level of PVDF, PE&PVDF will exhibit an emission spectrum (PVDF has an emission spectrum in $S1 \rightarrow S0$, and the electrons transition from S1 to S0 in orbitals of PVDF corresponding to photon emission); however, no emission spectrum is found in $S1 \rightarrow S0$

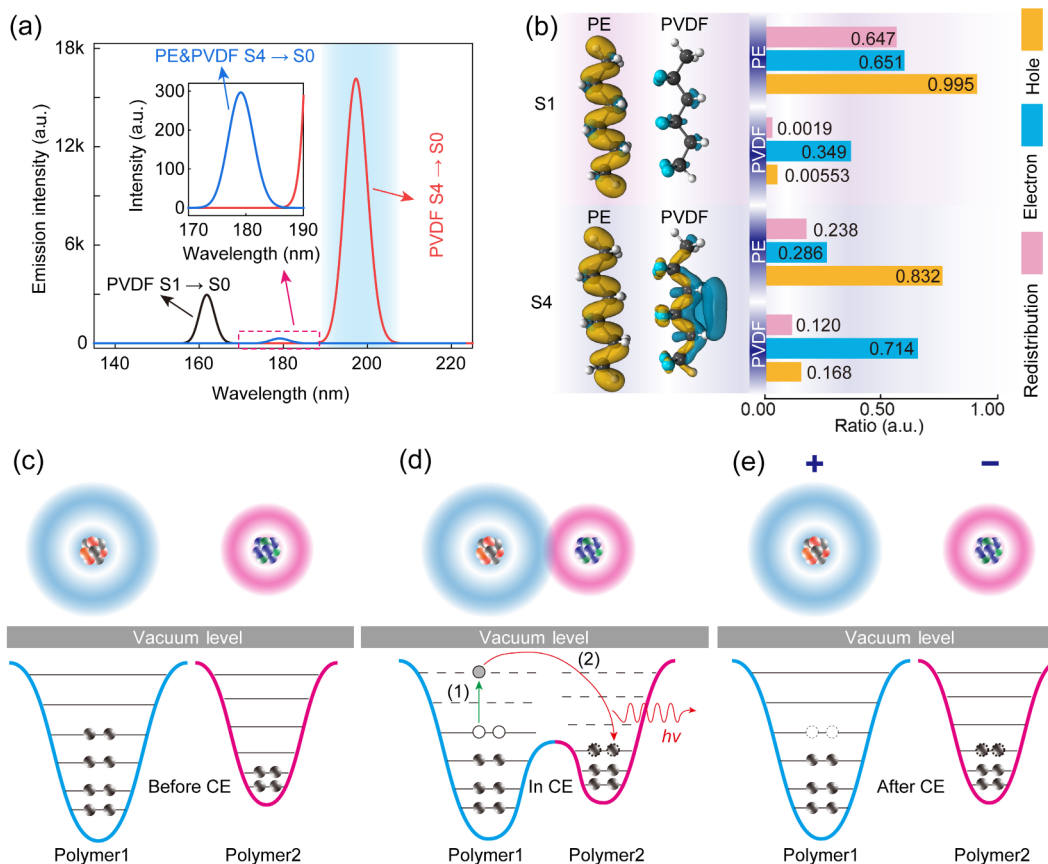


Figure 5 Contact electrification induced emission spectra and electron–hole analysis. (a) Emission spectra of PE, PVDF, and PE&PVDF at S1 and S4. (b) Analysis for the distributions of the electron (blue) and hole (yellow) for S1 and S4 of PE&PVDF in contact. Schematic diagrams of the physical process of electron transfer and CE induced interface spectra when two polymers are (c) before contact, (d) in contact, and (e) after contact.

when PE contacts with PVDF (Fig. 5(a)). As a result, the mechanism in which electrons are excited to the higher energy level of another material and then transitioned to a lower energy level is ruled out, as evidenced by the absence of an emission spectrum for PE&PET in S4 → S0 (Fig. 6(a)) and the absence of an emission spectrum of PE&PVDF in S4 → S0 (Fig. S10(a) in the ESM). Besides, if the emission spectrum of PE&PVDF in S4 → S0 is contributed by electrons that are excited to a higher energy level and followed by transitioning to a lower energy state of the PVDF, its main peak should locate in the same place as that of the emission spectrum of PVDF in S4 → S0 (Fig. 5(a)). The same peak position before and after contact can be seen in PE&PET in S1 → S0 (Fig. 6(a)), while the truth is that emission spectrum of PE&PET in S1 → S0 is actually the emission spectrum of PET, which is contributed by electronic structure rearrangement of PET. And the reduction in intensity is caused by partial electrons redistributed in PET being transferred to PE, but electron transfer in PE will not result in any emission spectrum. Furthermore, we discovered that the majority of PVDF electrons come from PE in S4, whereas electrons in PET at excited states come from redistribution in both S1 and S4. Hence, we can exclude the process that electrons are excited to the higher energy level and followed by transitioning to the lower energy level of the same material. As a result, the physical mechanism of CEIIPES must be that electrons are excited to a higher energy level in one material and then directly transitioned to a lower energy level of another material. This conclusion can also be confirmed by emission spectra and electron–hole analysis of PE&PP (S1 → S0) (Fig. S10 in the ESM) and PE&Kapton (S4 → S0) (Figs. S11(a) and S11(b) in the ESM). We also schematically summarized the mechanism of CEIIPES (Figs. 5(c)–5(e)). Electrons cannot transfer before the contact of two polymers because there is no electron cloud overlap

(Fig. 5(a)). When polymer1 contacts with polymer2, the electron clouds of two polymers overlap, resulting in electron transfer. And electrons transition during electron transfer due to CE, while the electrons at high energy levels are unstable and will transition to the lower energy level of another material. And the transition of electrons from a higher energy level of one material to the lower energy level of another material induced energy difference corresponding to photon emission according to Eq. (2), which will be detected in the experiment (Fig. 5(d)), this is the physical process of CEIIPES. After the separation of two polymers, polymer1 is positively charged and polymer2 is negatively charged (Fig. 5(c)).

Another scenario is that emission spectra are detected in the experiment as a result of electronic structure redistribution. To thoroughly investigate electron transition caused by CE, the origin of emission spectra must be identified. Similar to PVDF, emission spectra for PET are detected in S1 → S0 and S4 → S0, exhibiting diverse wavelengths and intensities, however the emission spectrum for PE&PET is only obtained in S1 → S0 (Fig. 6(a)). In contrast to the curve obtained by PE&PVDF contacting, the emission spectrum of PE&PET displays the same peak location as that of PET in S1 → S0, but its intensity is lower. It should be noticed that the excitation energy of PE&PET in S1 → S0 (3.635 eV) is similar to that of PET itself (3.632 eV). When combined with the derivative index of electron–hole analysis (Fig. 6(b)), electron excitation in S1 and S4 for PE&PET is mostly caused by electron transfer between two molecules. In terms of PE&PET, electron excitation is driven by the redistribution of PET in both S1 and S4, whereas the electrons in PE, albeit little, are provided by PET (Table S5 in the ESM). To better understand this process, we provided a graphic representation of the mechanism of emission spectra caused by electronic redistribution (Figs.

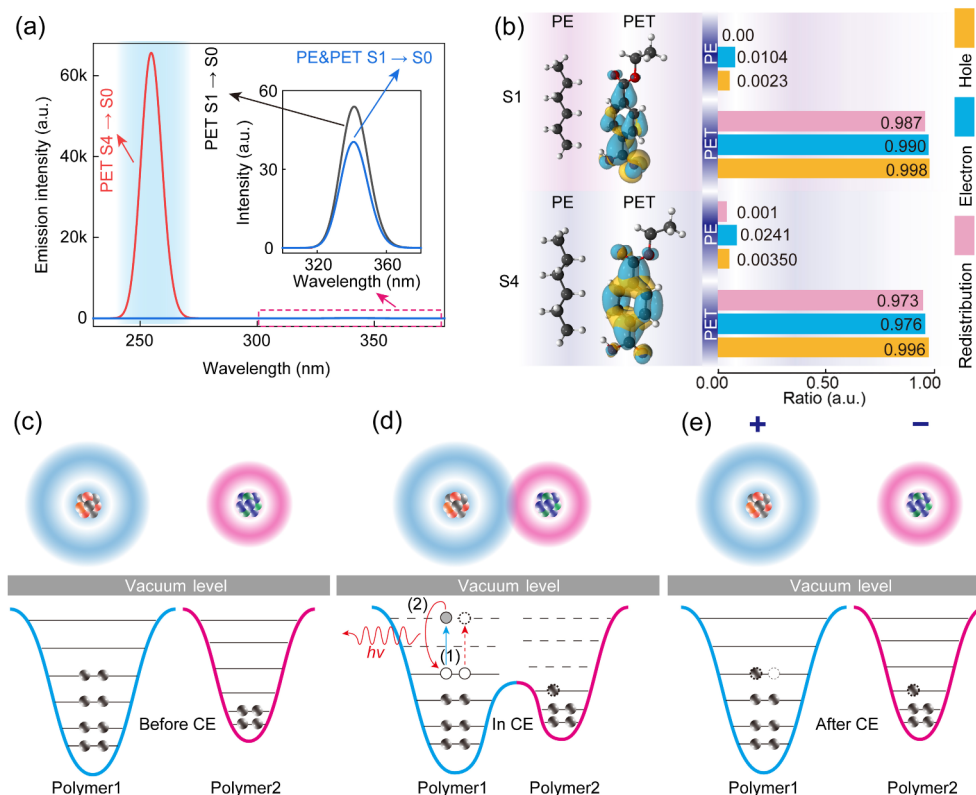


Figure 6 Electronic redistribution induced emission spectra and electron–hole analysis. (a) Emission spectra of PE, PET, and PE&PET at S1 and S4. (b) Analysis for the distributions of the electron (blue) and hole (yellow) for S1 and S4 of contacted PE&PET. Schematic diagrams of physical process of electron transfer and CE induced interface spectra when two polymers are (c) before contact, (d) in contact, and (e) after contact.

6(c)–6(e)). In addition to the electron transfer as mentioned above, some electrons are excited to a higher energy level due to CE or external factors, while electrons at high energy levels are unstable and will transition to a lower energy level of this material to redistribute electronic structure and make the contacted system stable. This process also causes energy differences and then induces photon emission, which will be detected as spectra in the experiment. Such emission spectra induced by electronic redistribution are also discoverable and provable in emission spectra and electron–hole analysis of PE&Kapton ($S1 \rightarrow S0$) and PE&Nylon66 ($S1 \rightarrow S0$), where the electron and hole are concentrated (Fig. S11 in the ESM). These emission spectra are comparable to those of individual materials. Differently, the amount of excited electrons that transition to lower energy levels will be altered by the electron transfer and transition during the CE process as compared with the case of only one material. This also explains that the absence of PE&PET emission spectrum in $S4 \rightarrow S0$ is due to the rearrangement of electronic structure. Therefore, CEIPES will have a distinct peak position when compared with the emission spectra of the individual materials. The aforementioned analyses suggest that both emission spectra during CE and of specific materials must be characterized in order to differentiate whether it is CEIPES or the emission spectrum of the material itself.

3 Conclusions

Through the methods of DFT and TDDFT, physical mechanisms of CEIPES and CEIIAS have been theoretically studied. The main conclusions can be summarized as follows:

(1) The direction of electron transfer across an interface has also been noticed, which has demonstrated to be a substantial relationship with the ESP. To describe these phenomena quantitatively, a new term R_{pn} was introduced and defined by $A_{\text{positive}}/A_{\text{negative}}$, where A_{positive} and A_{negative} represent the areas of

positive region and negative region of electrostatic surface potential, respectively. It is found that a larger value of R_{pn} means a stronger ability of obtaining electrons from another material during CE due to the attractive nature of the positive areas of ESP. This term can be utilized not only in the polymer/polymer system, but also for a CE system of polymer/metal. Moreover, we further confirmed that the electron transfer is proportional to the area of electron cloud overlap in particular in the case of parallel ordering and small contact distance. Therefore, the new term R_{pn} and electron cloud overlap model can be utilized simultaneously to clarify the electron transition process during CE.

(2) Except for the photon emission spectra during CE, the absorption spectra caused by the intermolecular electron transfer excitation were also predicted, which are regarded as CEIIAS. We find, quite interestingly, the main peak of the absorption spectrum at lower excited states (the first 5 excited states) is mainly contributed by electron transfer, while the main peak at higher excited states (the first 10 and the first 50 excited states) primarily stems from electrostatic structure rearrangement of the polymer itself. Against this background, it is then easily fitting to note that the absorption spectrum is dominated by electron transfer in a relatively lower excited states; while at the higher excited states, it is primarily contributed by the rearrangement of electrostatic structures. This evidence is revealed from the other side that the energy utilized for transferred electron transition introduced by CE is finite, making it difficult to excite the electrons to a high energy level.

(3) There are two mechanisms of CEIPES. During CE, the excited electrons from a higher energy level of one material are transferred/transmitted to a lower energy state of the other material, resulting in the phenomenon of photon emission. Another possible physical process of CEIPES is that some excited electrons at a higher energy level of one material are unstable, which will transfer/transmit to a lower energy state of this material to reach a stable CE system, thus leading to an electronic structure

redistribution and photon emission. Understanding how to distinguish between emission spectra generated by electron transfer and those created by electronic structure redistribution can help us to better understand the process of electronic transition in CE. This can be resolved by comparing the peak positions of emission spectra from two contacting materials during CE with those of individual materials, which were thoroughly investigated in this work. We anticipate that the efforts we have done could open up an avenue for developing modern spectroscopy based on CE.

4 Computational methods

4.1 General method

All DFT and TDDFT calculations were carried out by implementing the Gaussian 16 (C. 01) program package. The gas-phase ground state geometry optimizations were performed by using B3LYP exchange-correlation functional in conjunction with the 6-31G** basis set. In addition, the density functional dispersion correction was conducted by Grimme's D3 version with Becke–Johnson damping function. The TDDFT calculations were realized by implementing M06-2X exchange-correlation functional in conjunction with def2-TZVP basis set [46]. The electron transfer, electrostatic potential, absorption spectra, emission spectra, and electron–hole were analyzed by using Mutiwfn program (version 3.8) [47].

4.2 DFT calculations

All polymers were extensively optimized before being combined for additional optimization. Following the second optimization, each pair was subjected to a single point energy calculation for further consideration. To measure intermolecular electron transfer, the charges were estimated using atomic dipole moment corrected Hirshfeld atomic charges (ADCHs) [48], with the contacted polymers defined as fragment1 and fragment2, respectively. And the transferred electrons were estimated by means of comparing the charge of each fragment before and after contact. As for investigating the factors that influence the amount of electron transfer, each modified configuration (different orderings, different lengths, and different contact distances) performed the extra relaxation and single point energy calculations, where the changing distance between polymers necessitated the fixing of carbon atoms. Notably, we have not given the specific value of electron transfer when evaluating the transfer direction of all contact pairs (Fig. S3 in the ESM), because all polymers encompassed here were saturated, and the amount of electron transfer would be influenced by polymer ordering, polymer length, and distance, while these factors would not change the direction of electron transfer.

4.3 TDDFT calculations

The absorption spectra were obtained by calculating the vertical energy between the optimum ground state and the singlet excited states [18]. DFT calculations yielded optimum configurations. In addition, the emission spectra were obtained by calculating the vertical energy between the specific optimized singlet excited states and the ground state. We optimized all the contacted pairs mentioned in the DFT calculation from the lowest excited singlet state S1 to S5. Only the pairs that could be optimized in the specific excited state (like S1, S2, or others) were discussed. Furthermore, we chose these pairs optimized in the same excited state for discussion, for example, PE&PVDF and PE&PET both can be optimized in S1, which are comparable. However,

optimized PE&PVDF in S2 cannot be compared with optimized PE&PET in S3. Furthermore, we are unable to get optimum configurations of PTFE and PTFE related pairs, although the conclusions are unaffected.

Acknowledgements

This research was supported by the National Natural Science Foundation of China (Nos. 62001031, 52192610, 51702018, and 51432005), the Youth Innovation Promotion Association, CAS, the Fundamental Research Funds for the Central Universities (No. E0E48957), and the National Key R&D Program from Minister of Science and Technology (No. 2016YFA0202704). The authors are grateful to Xin-Zheng Li from Peking University of China for helpful discussions.

Electronic Supplementary Material: Supplementary material (configurations and electronic properties of all polymers, electron transfer data, supporting spectra, electron–hole analysis, and the definition of parameters related to computation) is available in the online version of this article at <https://doi.org/10.1007/s12274-023-5674-2>.

References

- [1] Herzberg, G. *Molecular Spectra and Molecular Structure*; D. van Nostrand: Princeton, 1945.
- [2] Morton, R. A. Spectroscopy as a biochemical tool. *Nature* **1962**, *193*, 314–318.
- [3] Day, D. E. Determining the Co-ordination number of aluminium ions by X-ray emission spectroscopy. *Nature* **1963**, *200*, 649–651.
- [4] Hachtel, J. A.; Huang, J. S.; Popovs, I.; Jansone-Popova, S.; Keum, J. K.; Jakowski, J.; Lovejoy, T. C.; Dellby, N.; Krivanek, O. L.; Idrobo, J. C. Identification of site-specific isotopic labels by vibrational spectroscopy in the electron microscope. *Science* **2019**, *363*, 525–528.
- [5] Barone, V.; Alessandrini, S.; Biczysko, M.; Cheeseman, J. R.; Clary, D. C.; McCoy, A. B.; DiRisio, R. J.; Neese, F.; Melosso, M.; Puzzarini, C. Computational molecular spectroscopy. *Nat. Rev. Methods Primers* **2021**, *1*, 38.
- [6] Bohr, N. XXXVII. On the constitution of atoms and molecules. *London Edinburgh Dublin Philos. Mag. J. Sci.* **1913**, *26*, 476–502.
- [7] Stefánsson, A.; Gunnarsson, I.; Giroud, N. New methods for the direct determination of dissolved inorganic, organic, and total carbon in natural waters by reagent-free™ ion chromatography and inductively coupled plasma atomic emission spectrometry. *Anal. Chim. Acta* **2007**, *582*, 69–74.
- [8] Mermet, J. M. Is it still possible, necessary, and beneficial to perform research in ICP-atomic emission spectrometry. *J. Anal. At. Spectrom.* **2005**, *20*, 11–16.
- [9] Li, D.; Xu, C.; Liao, Y. J.; Cai, W. Z.; Zhu, Y. Q.; Wang, Z. L. Interface inter-atomic electron-transition induced photon emission in contact-electrification. *Sci. Adv.* **2021**, *7*, eabj0349.
- [10] Wang, W. X.; Wang, Z. B.; Zhang, J. C.; Zhou, J. Y.; Dong, W. B.; Wang, Y. H. Contact electrification induced mechanoluminescence. *Nano Energy* **2022**, *94*, 106920.
- [11] Xie, Y. J.; Li, Z. Triboluminescence: Recalling interest and new aspects. *Chem* **2018**, *4*, 943–971.
- [12] Potashnik, R.; Goldschmidt, C. R.; Ottolenghi, M.; Weller, A. Absorption spectra of exciplexes. *J. Chem. Phys.* **1971**, *55*, 5344–5348.
- [13] Nam, K. H. Molecular dynamics-from small molecules to macromolecules. *Int. J. Mol. Sci.* **2021**, *22*, 3761.
- [14] Farr, E. P.; Quintana, J. C.; Reynoso, V.; Ruberry, J. D.; Shin, W. R.; Swartz, K. R. Introduction to time-resolved spectroscopy: Nanosecond transient absorption and time-resolved fluorescence of eosin B. *J. Chem. Educ.* **2018**, *95*, 864–871.
- [15] Louie, S. G.; Chan, Y. H.; da Jornada, F. H.; Li, Z. L.; Qiu, D. Y.



- Discovering and understanding materials through computation. *Nat. Mater.* **2021**, *20*, 728–735.
- [16] Fish, J.; Wagner, G. J.; Keten, S. Mesoscopic and multiscale modelling in materials. *Nat. Mater.* **2021**, *20*, 774–786.
- [17] Marzari, N.; Ferretti, A.; Wolverton, C. Electronic-structure methods for materials design. *Nat. Mater.* **2021**, *20*, 736–749.
- [18] Adamo, C.; Jacquemin, D. The calculations of excited-state properties with time-dependent density functional theory. *Chem. Soc. Rev.* **2013**, *42*, 845–856.
- [19] Petersilka, M.; Gossmann, U. J.; Gross, E. K. U. Excitation energies from time-dependent density-functional theory. *Phys. Rev. Lett.* **1996**, *76*, 1212–1215.
- [20] Runge, E.; Gross, E. K. U. Density-functional theory for time-dependent systems. *Phys. Rev. Lett.* **1984**, *52*, 997–1000.
- [21] Sun, M. Z.; Lu, Q. Y.; Wang, Z. L.; Huang, B. L. Understanding contact electrification at liquid–solid interfaces from surface electronic structure. *Nat. Commun.* **2021**, *12*, 1752.
- [22] Nan, Y.; Shao, J. J.; Willatzen, M.; Wang, Z. L. Understanding contact electrification at water/polymer interface. *Research* **2022**, *2022*, 9861463.
- [23] Xiang, Y. P.; Li, P.; Gong, S. L.; Huang, Y. H.; Wang, C. Y.; Zhong, C.; Zeng, W. X.; Chen, Z. X.; Lee, W. K.; Yin, X. J. et al. Acceptor plane expansion enhances horizontal orientation of thermally activated delayed fluorescence emitters. *Sci. Adv.* **2020**, *6*, eaba7855.
- [24] Tang, X.; Cui, L. S.; Li, H. C.; Gillett, A. J.; Auras, F.; Qu, Y. K.; Zhong, C.; Jones, S. T. E.; Jiang, Z. Q.; Friend, R. H. et al. Highly efficient luminescence from space-confined charge-transfer emitters. *Nat. Mater.* **2020**, *19*, 1332–1338.
- [25] Sun, L. L.; Lin, S. Q.; Tang, W.; Chen, X.; Wang, Z. L. Effect of redox atmosphere on contact electrification of polymers. *ACS Nano* **2020**, *14*, 17354–17364.
- [26] Wu, J.; Wang, X. L.; Li, H. Q.; Wang, F.; Yang, W. X.; Hu, Y. Q. Insights into the mechanism of metal-polymer contact electrification for triboelectric nanogenerator via first-principles investigations. *Nano Energy* **2018**, *48*, 607–616.
- [27] Pan, Q. Y.; Abdellah, M.; Cao, Y. H.; Lin, W. H.; Liu, Y.; Meng, J.; Zhou, Q.; Zhao, Q.; Yan, X. M.; Li, Z. L. et al. Ultrafast charge transfer dynamics in 2D covalent organic frameworks/Re-complex hybrid photocatalyst. *Nat. Commun.* **2022**, *13*, 845.
- [28] Cui, L. S.; Gillett, A. J.; Zhang, S. F.; Ye, H.; Liu, Y.; Chen, X. K.; Lin, Z. S.; Evans, E. W.; Myers, W. K.; Ronson, T. K. et al. Fast spin-flip enables efficient and stable organic electroluminescence from charge-transfer states. *Nat. Photonics* **2020**, *14*, 636–642.
- [29] Baytekin, H. T.; Patashinski, A. Z.; Branicki, M.; Baytekin, B.; Soh, S.; Grzybowski, B. A. The mosaic of surface charge in contact electrification. *Science* **2011**, *333*, 308–312.
- [30] Zou, H. Y.; Zhang, Y.; Guo, L. T.; Wang, P. H.; He, X.; Dai, G. Z.; Zheng, H. W.; Chen, C. Y.; Wang, A. C.; Xu, C. et al. Quantifying the triboelectric series. *Nat. Commun.* **2019**, *10*, 1427.
- [31] Lin, S. Q.; Xu, C.; Xu, L.; Wang, Z. L. The overlapped electron-cloud model for electron transfer in contact electrification. *Adv. Funct. Mater.* **2020**, *30*, 1909724.
- [32] Xu, C.; Zi, Y. L.; Wang, A. C.; Zou, H. Y.; Dai, Y. J.; He, X.; Wang, P. H.; Wang, Y. C.; Feng, P. Z.; Li, D. W. et al. On the electron-transfer mechanism in the contact-electrification effect. *Adv. Mater.* **2018**, *30*, 1706790.
- [33] Wang, Z. L. Triboelectric nanogenerator (TENG)-sparking an energy and sensor revolution. *Adv. Energy Mater.* **2020**, *10*, 2000137.
- [34] Wang, Z. L.; Wang, A. C. On the origin of contact-electrification. *Mater. Today* **2019**, *30*, 34–51.
- [35] Yoshida, M.; Ii, N.; Shimosaka, A.; Shirakawa, Y.; Hidaka, J. Experimental and theoretical approaches to charging behavior of polymer particles. *Chem. Eng. Sci.* **2006**, *61*, 2239–2248.
- [36] Shirakawa, Y.; Ii, N.; Yoshida, M.; Takashima, R.; Shimosaka, A.; Hidaka, J. Quantum chemical calculation of electron transfer at metal/polymer interfaces. *Adv. Powder Technol.* **2010**, *21*, 500–505.
- [37] Liu, C. Y.; Bard, A. J. Electrons on dielectrics and contact electrification. *Chem. Phys. Lett.* **2009**, *480*, 145–156.
- [38] Pan, S. H.; Zhang, Z. N. Triboelectric effect: A new perspective on electron transfer process. *J. Appl. Phys.* **2017**, *122*, 144302.
- [39] McCarty, L. S.; Whitesides, G. M. Electrostatic charging due to separation of ions at interfaces: Contact electrification of ionic electrets. *Angew. Chem., Int. Ed.* **2008**, *47*, 2188–2207.
- [40] McCarty, L. S.; Winkleman, A.; Whitesides, G. M. Ionic electrets: Electrostatic charging of surfaces by transferring mobile ions upon contact. *J. Am. Chem. Soc.* **2007**, *129*, 4075–4088.
- [41] Lowell, J. The role of material transfer in contact electrification. *J. Phys. D Appl. Phys.* **1977**, *10*, L233–L235.
- [42] Baytekin, H. T.; Baytekin, B.; Incorvati, J. T.; Grzybowski, B. A. Material transfer and polarity reversal in contact charging. *Angew. Chem., Int. Ed.* **2012**, *51*, 4843–4847.
- [43] Liu, Z. Y.; Wang, X.; Lu, T.; Yuan, A. H.; Yan, X. F. Potential optical molecular switch: Lithium@cyclo[18]carbon complex transforming between two stable configurations. *Carbon* **2022**, *187*, 78–85.
- [44] Jacquemin, D.; Planchat, A.; Adamo, C.; Mennucci, B. TD-DFT assessment of functionals for optical 0–0 transitions in solvated dyes. *J. Chem. Theory Comput.* **2012**, *8*, 2359–2372.
- [45] Liu, Z. Y.; Lu, T.; Chen, Q. X. An sp-hybridized all-carboatomic ring, cyclo[18]carbon: Electronic structure, electronic spectrum, and optical nonlinearity. *Carbon* **2020**, *165*, 461–467.
- [46] Weigend, F.; Ahlrichs, R. Balanced basis sets of split valence, triple zeta valence, and quadruple zeta valence quality for H to Rn: Design and assessment of accuracy. *Phys. Chem. Chem. Phys.* **2005**, *7*, 3297–3305.
- [47] Lu, T.; Chen, F. W. Multiwfn: A multifunctional wavefunction analyzer. *J. Comput. Chem.* **2012**, *33*, 580–592.
- [48] Lu, T.; Chen, F. W. Atomic dipole moment corrected Hirshfeld population method. *J. Theor. Comput. Chem.* **2012**, *11*, 163–183.